Roles of RIG-I N-terminal tandem CARD and splice variant in TRIM25-mediated antiviral signal transduction

Michaela U. Gack*[†‡], Axel Kirchhofer[§], Young C. Shin[†], Kyung-Soo Inn*[†], Chengyu Liang*[†], Sheng Cui[§], Sua Myong[¶], Taekjip Ha[¶], Karl-Peter Hopfner[§], and Jae U. Jung*[†‖]

*Department of Molecular Microbiology and Immunology, Keck School of Medicine, University of Southern California, Harlyne J. Norris Cancer Research Tower, 1450 Biggy Street, Los Angeles, CA 90033; [†]Department of Microbiology and Molecular Genetics and Tumor Virology Division, New England Primate Research Center, Harvard Medical School, 1 Pine Hill Drive, Southborough, MA 01772; [‡]Institute for Clinical and Molecular Virology, Friedrich Alexander University Erlangen–Nuremberg, Schlossgarten 4, 91054 Erlangen, Germany; [§]Gene Center and Center for Integrated Protein Science, Department of Chemistry and Biochemistry, Ludwig Maximilians University of Munich, Feodor-Lynen-Strasse 25, 81377 Munich, Germany; and [¶]Department of Physics, University of Illinois at Urbana–Champaign, Room 133, Loomis Laboratory, MC 704, 1110 West Green Street, Urbana, IL 61801

Edited by Peter Palese, Mount Sinai School of Medicine, New York, NY, and approved September 2, 2008 (received for review May 21, 2008)

The caspase recruitment domain (CARD) of intracellular adaptors and sensors plays a critical role in the assembly of signaling complexes involved in innate host defense against pathogens and in the regulation of inflammatory responses. The cytosolic receptor retinoic acid-inducible gene-I (RIG-I) recognizes viral RNA in a 5′-triphosphate-dependent manner and initiates an antiviral signaling cascade. Upon viral infection, the N-terminal CARDs of RIG-I undergo the K_{63}-linked ubiquitination induced by tripartite motif protein 25 (TRIM25), critical for the interaction of RIG-I with its downstream signaling partner MAVS/VISA/IPS-1/Cardif. Here, we demonstrate the distinct roles of RIG-I first and second CARD in TRIM25-mediated RIG-I ubiquitination: TRIM25 binds the RIG-I first CARD and subsequently ubiquitinates its second CARD. The $T_{55}I$ mutation in RIG-I first CARD abolishes TRIM25 interaction, whereas the $K_{172}R$ mutation in the second CARD eliminates polyubiquitin attachment. The necessity of the intact tandem CARD for RIG-I function is further evidenced by a RIG-I splice variant (SV) whose expression is robustly up-regulated upon viral infection. The RIG-I SV carries a short deletion (amino acids 36–80) within the first CARD and thereby loses TRIM25 binding, CARD ubiquitination, and downstream signaling ability. Furthermore, because of its robust inhibition of virus-induced RIG-I multimerization and RIG-I-MAVS signaling complex formation, this SV effectively suppresses the RIG-I-mediated IFN-β production. This study not only elucidates the vital role of the intact tandem CARD for TRIM25-mediated RIG-I activation but also identifies the RIG-I SV as an off-switch regulator of its own signaling pathway.

alternative splicing | innate immunity | interferon

The caspase recruitment domain (CARD)-containing intracellular sensors, RIG-I, melanoma differentiation-associated gene 5 (MDA5), and nucleotide-binding and oligomerization domain (NOD), play important roles in the detection of conserved molecular structures of invading microbes (1–4). Specifically, RIG-I and MDA5 function as cytosolic receptors for viral 5′-triphosphate single-stranded RNA and double-stranded RNA (dsRNA), respectively, whereas NOD1 and NOD2 act as intracellular sensors for bacterial peptidoglycans (5–8). Upon ligand binding and activation, these intracellular pattern recognition receptors (PRRs) interact through their CARDs with downstream CARD-containing molecules to ultimately initiate a signaling cascade, resulting in the production of IFN-α/β and inflammatory cytokines to limit viral or bacterial proliferation (9, 10).

RIG-I and MDA5 consist of two N-terminal CARDs, a central DECH box ATPase domain, and a C-terminal regulatory/repressor domain (RD) (11, 12). Whereas the C-terminal RD of RIG-I binds viral RNA in a 5′-triphosphate-dependent manner and activates the central ATPase by RNA-dependent dimerization (13, 14), the CARDs of RIG-I trigger the interaction with its downstream partner MAVS/VISA/IPS-1/Cardif (15–18). The crucial role of the tandem CARD for RIG-I downstream signaling is further evidenced by the finding that the hepatocyte cell line Huh7.5, which carries the $T_{55}I$ mutation in the RIG-I first CARD, strongly supports hepatitis C virus (HCV) replication (19). The $T_{55}I$ mutation disrupts the signaling function of the RIG-I CARDs to induce antiviral IFN production, leading to a high permissiveness to HCV replication. Furthermore, we have recently shown that the CARDs of RIG-I interact with the C-terminal SPRY domain of tripartite motif 25 (TRIM25) E3 ligase, and this interaction effectively delivers the K63-linked ubiquitin moieties to the RIG-I second CARD, resulting in a marked increase of RIG-I downstream signaling activity (20). RIG-I Lys-172 (K_{172}) is critical for TRIM25-mediated ubiquitination and MAVS/VISA/IPS-1/Cardif binding, as well as the ability of RIG-I to induce antiviral signal transduction.

Unbalanced, continuous production of IFNs and inflammatory cytokines could lead to deleterious effects on host immunity. To tightly regulate the on/off switch of RIG-I-mediated innate immunity, RIG-I activity is negatively regulated by several mechanisms, including K48-linked ubiquitination leading to RIG-I degradation (21) and the LGP2 helicase protein, which lacks the N-terminal CARDs (22, 23). In addition, alternative splicing has been identified as an important cellular regulatory mechanism in fine-tuning host IFN signaling activity. For instance, the alternatively spliced variants of NOD2 and MyD88 function as dominant-negative inhibitors of NOD2 and TLR-induced signal transduction, respectively (24–26).

Here, we describe the distinct roles of the CARDs of RIG-I for TRIM25-binding and TRIM25-mediated ubiquitination and identify an alternatively spliced variant of RIG-I as a potential feedback inhibitor of its signal transduction, thereby unveiling the intricate regulation of RIG-I-mediated antiviral innate immunity.

Results

Distinct Roles of the RIG-I First and Second CARD in TRIM25-Mediated RIG-I Ubiquitination. To define the functions of the RIG-I first and second CARD in TRIM25-RIG-I-complex formation and TRIM25-mediated RIG-I activation, GST-RIG-I first CARD, GST-RIG-I second CARD, and GST-RIG-I 2CARD mammalian

Author contributions: M.U.G., Y.C.S., K.-S.I., C.L., K.-P.H., and J.U.J. designed research; M.U.G., A.K., and S.C. performed research; S.M. and T.H. contributed new reagents/analytic tools; M.U.G., A.K., Y.C.S., K.-S.I., C.L., and S.C. analyzed data; and M.U.G. wrote the paper.

The authors declare no conflict of interest.

This article is a PNAS Direct Submission.

‖To whom correspondence should be addressed. E-mail: jaeujung@usc.edu.

This article contains supporting information online at www.pnas.org/cgi/content/full/0804947105/DCSupplemental.

MICROBIOLOGY

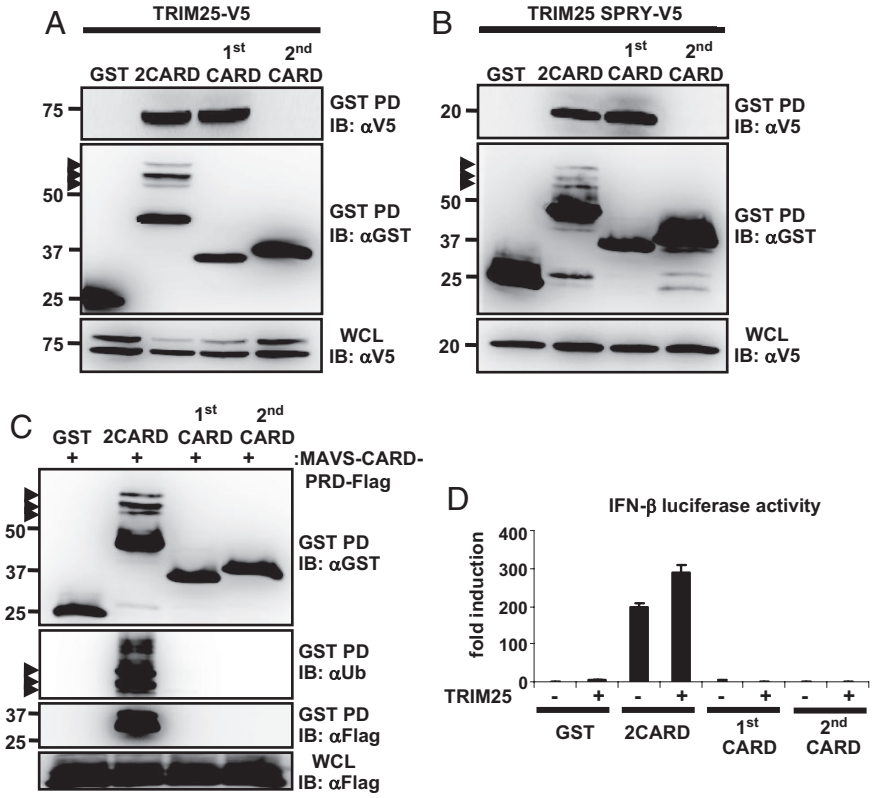

Fig. 1. The intact tandem CARD of RIG-I is essential for TRIM25-mediated RIG-I activation. (*A* and *B*) TRIM25 interaction with RIG-I first CARD. HEK293T cells were transfected with GST, GST-RIG-I 2CARD, GST-RIG-I first CARD, or GST-RIG-I second CARD together with TRIM25-V5 (*A*) or TRIM25-SPRY-V5 (*B*). Whole-cell lysates (WCLs) were subjected to GST-pulldown (GST-PD), followed by immunoblotting (IB) with α-V5 or α-GST. Arrows indicate the ubiquitinated bands. (*C*) Both CARDs are necessary for RIG-I ubiquitination and interaction with MAVS. At 48 h after transfection with GST, GST-RIG-I 2CARD, GST-RIG-I first CARD, or GST-RIG-I second CARD together with MAVS-CARD-PRD-Flag, HEK293T WCLs were used for GST-PD, followed by IB with α-GST, α-Ub, or α-Flag. (*D*) Both CARDs are necessary for TRIM25-mediated RIG-I signaling. GST-RIG-I fusion constructs with or without TRIM25 together with IFN-β luciferase and constitutive β-gal-expressing pGK-β-gal were expressed in HEK293T cells. Luciferase and β-galactosidase values were determined as described (20). Data represent the mean ± SD ($n = 3$).

fusion constructs were tested for TRIM25 binding. GST-pulldown indicated that GST-RIG-I first CARD and GST-RIG-I 2CARD strongly bound full-length TRIM25 and TRIM25-SPRY, whereas GST and GST-RIG-I second CARD showed no interactions (Fig. 1 *A* and *B*). Regardless of TRIM25 binding, however, neither GST-RIG-I first CARD nor GST-RIG-I second CARD showed any detectable level of ubiquitination and MAVS-CARD-proline-rich-domain (PRD) interaction, whereas GST-RIG-I 2CARD underwent robust ubiquitination and efficiently interacted with MAVS-CARD-PRD under the same conditions [Fig. 1*C* and supporting information (SI) Fig. S1*A*]. In correlation with their lack of ubiquitination and MAVS binding, each CARD of RIG-I was incapable of activating the IFN-β and NF-κB promoters (Fig. 1*D* and Fig. S1*B*). These results indicate that, whereas the first CARD is responsible for TRIM25 binding, the intact tandem CARD of RIG-I is necessary for TRIM25-mediated ubiquitination, ultimately allowing efficient MAVS interaction and downstream signal transduction.

Threonine 55 Residue of the RIG-I First CARD Is Critical for TRIM25 Binding. The $T_{55}I$ mutation of RIG-I first CARD abolishes RIG-I-mediated antiviral activity, leading to a high permissiveness to HCV replication (19). However, the molecular mechanism by which the $T_{55}I$ mutation abrogates RIG-I-mediated antiviral signal transduction has not yet been illustrated. We found that the RIG-I $T_{55}I$ mutation abolished its TRIM25 binding ability, leading to the loss of TRIM25-induced RIG-I ubiquitination (Fig. 2 *A* and *B* and Fig. S2*A*). Consistently, ectopic expression of TRIM25 efficiently enhanced the activity of GST-RIG-I 2CARD WT but not GST-RIG-I 2CARD $T_{55}I$ in inducing IFN-β promoter activation (Fig. 2*C*). To examine the capability of RIG-I 2CARD $T_{55}I$ for interacting with MAVS, several previously described (20) GST-RIG-I 2CARD mutants were included in this assay: GST-RIG-I 2CARD $K_{172}R$, in which the main ubiquitination site is mutated, GST-RIG-I 2CARD $K_{99/169/172/181/190/193}R$, in which all six ubiquitination sites are mutated, and GST-RIG-I 2CARD $K_{172only}$, containing five $K \rightarrow R$ substitutions while leaving K_{172} intact (Fig. 2*D*). GST-RIG-I 2CARD $T_{55}I$, $K_{172}R$, and $K_{99/169/172/181/190/193}R$ mutants that did not undergo ubiquitination bound poorly to MAVS-CARD-PRD, whereas GST-RIG-I 2CARD WT and $K_{172only}$, which were heavily ubiquitinated, interacted strongly with MAVS-CARD-PRD (Fig. 2*D*). This indicates that TRIM25-mediated ubiquitination of RIG-I is necessary for efficient interaction with MAVS. Indeed, MAVS-CARD-PRD displayed a higher binding affinity to the ubiquitinated form of the RIG-I 2CARD than the unmodified form (Fig. S2*B*). Furthermore, shRNA-mediated TRIM25 knockdown markedly suppressed the interaction between RIG-I 2CARD and MAVS-CARD-PRD (Fig. S2*C*). These results demonstrate that the T_{55} residue of the RIG-I first CARD is critical for TRIM25 binding and subsequently TRIM25-mediated ubiquitination, which is ultimately necessary for efficient RIG-I-MAVS interaction.

Because the T_{55} or S_{55} residue of RIG-I is highly conserved among various species, the potential phosphorylation of this residue might trigger TRIM25 interaction. To test this hypothesis, we introduced a series of point mutations in place of T_{55}: $T_{55}E$ to mimic constitutive phosphorylation and $T_{55}I$, $T_{55}A$, and $T_{55}Q$ to mimic nonphosphorylation. The GST-RIG-I 2CARD mutants were then tested for TRIM25 binding, ubiquitination, and downstream signaling activity (Fig. 2 *E* and *F*). As shown in Fig. 2*E*, GST-RIG-I 2CARD $T_{55}Q$ and $T_{55}E$ exhibited an apparent reduction of TRIM25 binding and ubiquitination compared with GST-RIG-I 2CARD WT, whereas GST-RIG-I 2CARD $T_{55}A$ showed a similar extent of TRIM25 binding and ubiquitination compared with GST-RIG-I 2CARD WT. Furthermore, mass spectrometry analysis of purified GST-RIG-I 2CARD WT in the presence of phosphatase inhibitors showed no detectable phosphorylation or other known modifications at the T_{55} residue (data not shown). In addition, the levels of TRIM25 binding and ubiquitination of these mutants directly correlated with their ability to induce IFN-β and NF-κB promoter activation (Fig. 2*F*).

Given that mutation of the RIG-I T_{55} residue to the hydrophobic amino acid isoleucine abolished TRIM25 interaction, CARD ubiq-

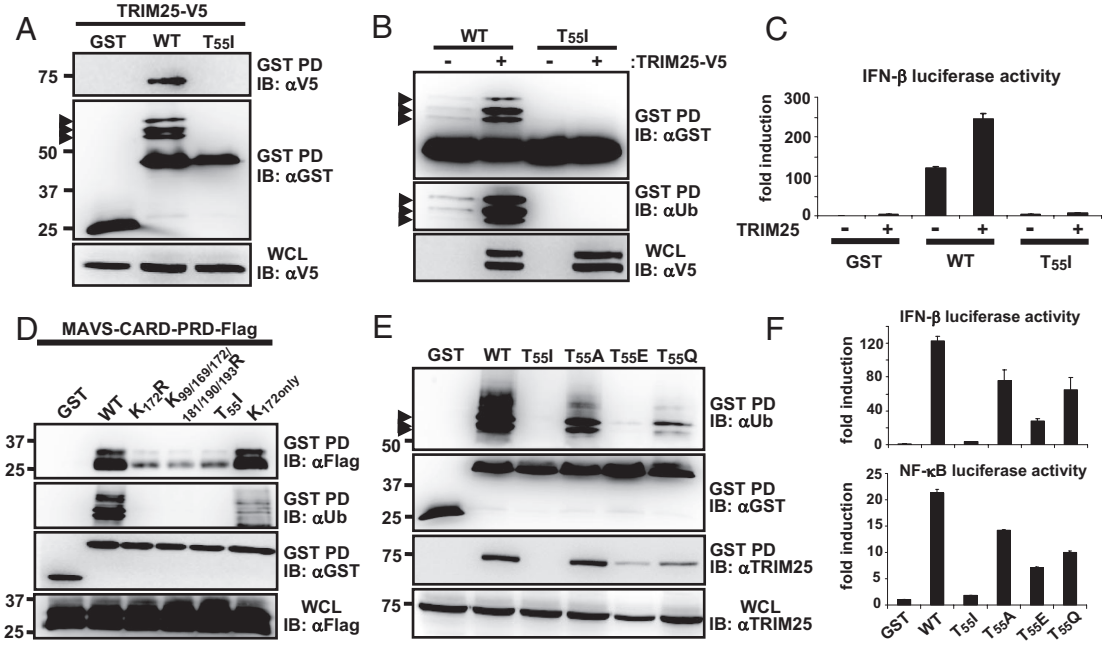

Fig. 2. The T_{55} residue of RIG-I is critical for TRIM25 binding. (*A*) T_{55}I mutation abolishes RIG-I-TRIM25-interaction. At 48 h after transfection with GST, GST-RIG-I 2CARD WT, or GST-RIG-I 2CARD T_{55}I together with TRIM25-V5 WCLs were used for GST-PD, followed by IB with α-V5 or α-GST. Arrows indicate the ubiquitinated bands. (*B* and *C*) T_{55}I mutation abolishes RIG-I CARD ubiquitination and downstream signaling. GST-RIG-I 2CARD WT or GST-RIG-I 2CARD T_{55}I with or without TRIM25-V5 was expressed in HEK293T. WCLs were used for GST-PD, followed by IB with α-GST or α-Ub. Arrows indicate the ubiquitinated bands. (*C*) GST-RIG-I 2CARD WT or T_{55}I with or without TRIM25 together with IFN-β luciferase and pGK-β-gal were expressed in HEK293T cells as described in Fig. 1*D*. Data represent the mean ± SD ($n = 3$). (*D*) T_{55}I mutation strongly decreases RIG-I binding to MAVS. HEK293T were transfected with MAVS-CARD-PRD-Flag together with GST or GST-RIG-I 2CARD fusion constructs. WCLs were subjected to GST-PD, followed by IB with α-Flag, α-Ub, or α-GST. MAVS-CARD-PRD expression was determined by IB with α-Flag. (*E* and *F*) Ubiquitination, TRIM25 binding, and signaling activity of RIG-I 2CARD T_{55} mutants. GST or GST-RIG-I 2CARD was expressed in HEK293T cells. WCLs were subjected to GST-PD, followed by IB with α-Ub, α-GST, or α-TRIM25. Arrows indicate the ubiquitinated bands. Luciferase assay was performed as described in Fig. 1*D*. Data represent the mean ± SD ($n = 3$).

uitination, and RIG-I downstream signaling, we addressed whether altering hydrophobicity at the T_{55} residue might interfere with TRIM25 binding and RIG-I signaling. Accordingly, the T_{55} residue of RIG-I was replaced with tryptophan (T_{55}W) or valine (T_{55}V). GST-RIG-I 2CARD T_{55}W and GST-RIG-I 2CARD T_{55}V showed no detectable TRIM25 binding or ubiquitination and exhibited a near complete loss of signaling activity in inducing IFN-β or NF-κB promoter activation (Fig. S3 *A* and *B*). These results collectively indicate that the lack of antiviral activity of the RIG-I T_{55}I mutant is due to the loss of its ability to bind TRIM25.

Identification of RIG-I SV. Given that the RIG-I first and second CARD are essential for TRIM25 binding and TRIM25-mediated ubiquitin attachment, respectively, we postulated that alternative splicing in the N-terminal tandem CARD of RIG-I might affect its ubiquitination-dependent signaling function. To test this hypothesis, we isolated total RNAs from mock- or IFN-β-treated HEK293T cells and performed RT-PCR using primers that specifically amplified the RIG-I CARDs (exons 1–3) (Fig. 3*B Upper*). In addition to the band corresponding to the expected size for the RIG-I CARDs sequence (735 bp), a band with a smaller size (603 bp) was detected in IFN-β-treated, but not in mock-treated HEK293T cells (Fig. 3*B*). Cloning and sequence analysis of the smaller amplicon identified a RIG-I SV that lacked the exon 2, coding for amino acids 36–80 of RIG-I. Additional RT-PCR analysis using primers to specifically amplify the complete ORF of RIG-I (exons 1–18) also identified the alternatively spliced variant of RIG-I carrying the deletion of exon 2 (Fig. 3*A*).

We further tested the expression patterns of full-length RIG-I and the SV in mock-treated versus IFN-β-treated or Sendai virus (SeV)-infected HEK293T cells, using primers specific for full-length RIG-I or the SV (Fig. 3*B* and Fig. S4*A*). Whereas a low level of full-length RIG-I mRNA was detected in mock-treated cells, the RIG-I SV was undetectable under the same conditions (Fig. 3*B* and Fig. S4*A*). Furthermore, the transcript levels of both full-length RIG-I and the SV significantly increased upon IFN-β treatment or SeV infection. Additionally, the RIG-I SV was detectable in a number of cell lines upon IFN-β treatment, including lymphatic endothelial cells (LECs), HeLa, HCT116, Huh7, LnCap, and NHLF lung fibroblast cells, but not after treatment with *all-trans* retinoic acid (Figs. S4*B* and S5*A*), indicating an IFN stimulation-specific expression of the RIG-I SV. In line with this, the RIG-I SV was readily detectable in 2fTGH WT human fibroblasts but not in STAT1-deficient (U3A) nor STAT2-deficient (U6A) cells upon treatment with IFN-α or IFN-β (Fig. S5*B*). Furthermore, a monoclonal RIG-I antibody that reacted with the central helicase domain readily detected a 100-kDa band in addition to the 116-kDa band corresponding to full-length RIG-I in IFN-β-treated or SeV-infected HEK293T cells but not in mock-treated cells (Fig. 3*B* and Fig. S4*A*). This 100-kDa band comigrated with exogenously expressed Flag-tagged RIG-I SV (Fig. S4*A*). Furthermore, a RIG-I antibody generated by the peptide containing residues 37–55 detected the 116-kDa full-length RIG-I but not the 100-kDa SV (Fig. S4*C*). These results indicate that RIG-I undergoes alternative splicing upon IFN stimulation, resulting in an isoform that lacks the short sequence of the first CARD containing the T_{55} residue.

Lack of TRIM25 Binding, Ubiquitination, and Signaling Activity of RIG-I SV. To study the potential role of the RIG-I SV in antiviral signal transduction, GST-RIG-I 2CARD SV was tested for a series of biochemical activities: TRIM25 binding, ubiquitination, MAVS binding, and downstream signal transducing ability. Like the GST-RIG-I 2CARD T_{55}I mutant (Fig. 2), GST-RIG-I 2CARD SV was unable to bind TRIM25 full-length and TRIM25-SPRY at detect-

MICROBIOLOGY

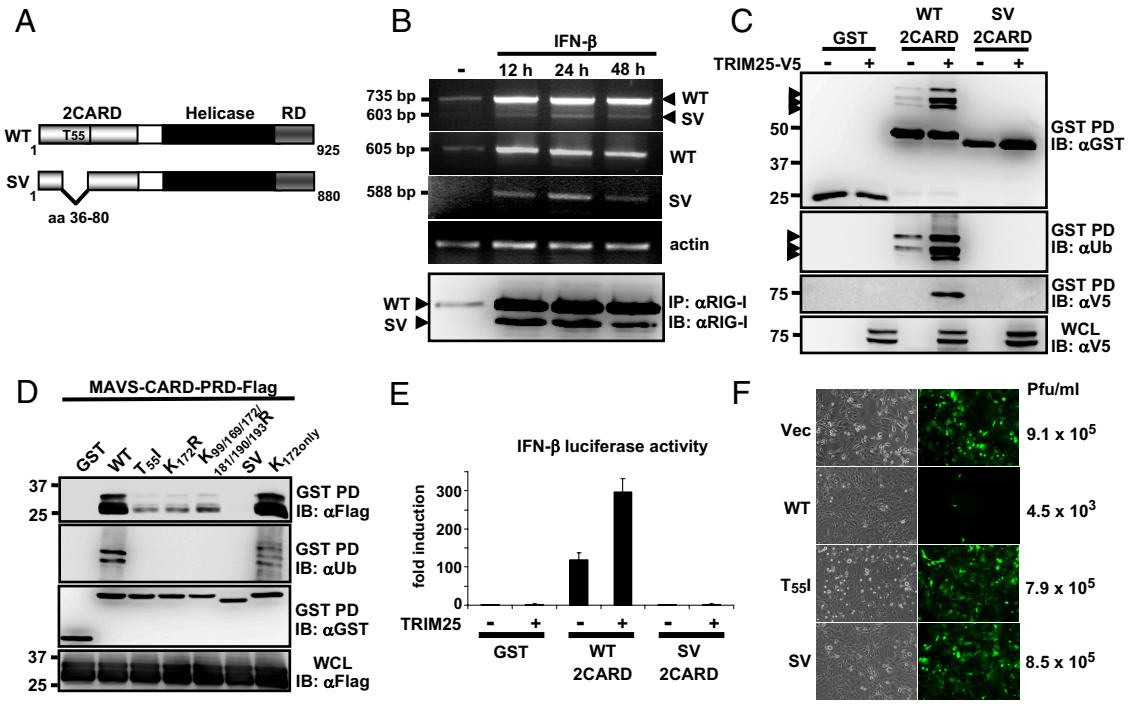

Fig. 3. Identification and biochemical characterization of RIG-I SV. (*A*) Schematic protein representations of RIG-I full-length and SV. (*B*) Transcript (*Upper*) and protein (*Lower*) of RIG-I SV. HEK293T cells were mock-treated or stimulated with IFN-β (1,000 units/ml) for the indicated number of hours. Total RNA was subjected to RT-PCR to amplify the RIG-I CARDs (exon 1–3). Transcript levels of RIG-I and RIG-I SV were further determined by using specific primers. The actin transcript was used as a control. RIG-I full-length and SV levels were determined with α-RIG-I. (*C*) Lack of TRIM25 binding and CARD ubiquitination of RIG-I SV. After transfection with GST, GST-RIG-I 2CARD WT, or GST-RIG-I 2CARD SV with or without TRIM25-V5, HEK293T WCLs were used for GST-PD, followed by IB with α-GST, α-Ub, or α-V5. Arrows indicate the ubiquitinated bands. (*D*) RIG-I SV does not interact with MAVS. At 48 h after transfection with MAVS-CARD-PRD-Flag and GST-RIG-I 2CARD, HEK293T WCLs were used for GST-PD, followed by IB with α-Flag, α-Ub, or α-GST. (*E*) Lack of signaling activity of RIG-I SV. HEK293T cells were transfected with GST, GST-RIG-I 2CARD WT, or GST-RIG-I 2CARD SV with or without TRIM25-V5 together with IFN-β luciferase and pGK-β-gal. Data represent the mean ± SD (n = 3). (*F*) Abolished antiviral function of RIG-I SV. RIG-I, RIG-I SV, or RIG-I T_{55}I mutant was stably expressed in RIG-$I^{-/-}$ MEFs, and these cells were infected with VSV-eGFP at MOI 0.5. At 40 h after infection, virus titer and replication were determined by plaque assay and GFP expression, respectively. Pfu, plaque-forming unit.

able levels and did not undergo TRIM25-mediated ubiquitination (Fig. 3*C* and Fig. S6*A*). Consistently, full-length RIG-I SV showed no detectable TRIM25 binding and extremely low K_{63}-linked ubiquitination (Fig. S6 *B* and *C*). Furthermore, whereas GST-RIG-I 2CARD T_{55}I, K_{172}R or $K_{99/169/172/181/190/193}$R mutants bound poorly to MAVS-CARD-PRD compared with GST-RIG-I 2CARD WT, GST-RIG-I 2CARD SV showed no interaction with MAVS-CARD-PRD (Fig. 3*D*). Finally, GST-RIG-I 2CARD SV was incapable of inducing IFN-β or NF-κB promoter activation in the presence or absence of exogenous TRIM25 (Fig. 3*E* and Fig. S6*D*).

To further test the antiviral activity of the RIG-I SV upon viral infection, we tested the replication of enhanced-GFP-containing vesicular stomatitis virus (VSV-eGFP) in RIG-$I^{-/-}$ mouse embryonic fibroblasts (MEFs) expressing vector, RIG-I WT, RIG-I SV, or RIG-I T_{55}I mutant. RIG-I WT expression drastically suppressed VSV-eGFP replication: VSV-eGFP titer was ≈200-fold lower in RIG-I WT-expressing cells than in vector-containing cells (Fig. 3*F*). In contrast, MEFs expressing the RIG-I SV or RIG-I T_{55}I mutant had similar viral titers to MEFs expressing vector only (Fig. 3*F*). Thus, the RIG-I SV, lacking a critical part of the first CARD, loses TRIM25 binding, which subsequently abolishes TRIM25-mediated ubiquitination and MAVS binding and, thereby, antiviral activity.

RIG-I SV Acts as a Dominant Inhibitor of RIG-I-Mediated Antiviral IFN Response. To explore the effects of the RIG-I SV on RIG-I signal transduction, HEK293T cells were transfected with IFN-β or NF-κB promoter luciferase together with increasing amounts of Flag-RIG-I SV, followed by SeV infection (Fig. 4*A* and Fig. S7). RIG-I T_{55}I mutant was included as a control. Although both RIG-I SV and RIG-I T_{55}I mutant markedly suppressed the SeV-induced IFN-β or NF-κB promoter activation, the level of suppression induced by RIG-I SV was markedly stronger than that induced by RIG-I T_{55}I mutant (Fig. 4*A* and Fig. S7). In addition, the exogenously expressed RIG-I SV potently inhibited SeV-induced IFN-β promoter activation in HCT116, Huh7, and HeLa cells (Fig. S8).

To further delineate the inhibitory effect of the RIG-I SV on the RIG-I-mediated downstream signaling cascade, we examined virus-induced phosphorylation, dimerization, and nuclear translocation of IFN regulatory factor 3 (IRF3). HEK293T cells were cotransfected with Myc-tagged RIG-I WT together with vector, Flag-RIG-I SV or RIG-I T_{55}I mutant followed by SeV infection. This showed that SeV infection led to a considerable shift of endogenous IRF3 to the slow-migrating phosphorylated forms that were also readily detected by anti-S_{396} phospho-specific IRF3 antibody (Fig. 4*B*). In contrast, ectopic expression of RIG-I SV and RIG-I T_{55}I mutant strongly suppressed the SeV-induced phosphorylation of IRF3 (Fig. 4*B*). In addition, RIG-I SV and RIG-I T_{55}I mutant almost completely blocked SeV-induced IRF3 dimerization (Fig. 4*C*). We further tested the nuclear translocation of IRF3-eGFP induced by SeV infection in HEK293T stably expressing vector, RIG-I WT, RIG-I SV, or RIG-I T_{55}I mutant. Although the nuclear translocation of IRF3-eGFP was apparently detected in HEK293T cells expressing vector or RIG-I WT upon SeV infection, it was not observed in cells expressing RIG-I SV or RIG-I T_{55}I mutant (Fig. 4*D*). Finally, RIG-I SV and RIG-I T_{55}I mutant expression detectably increased VSV-eGFP replication compared with vector expression. In contrast, RIG-I WT expression markedly decreased VSV-eGFP replication (Fig. 4*E*). Furthermore, HEK293T cells

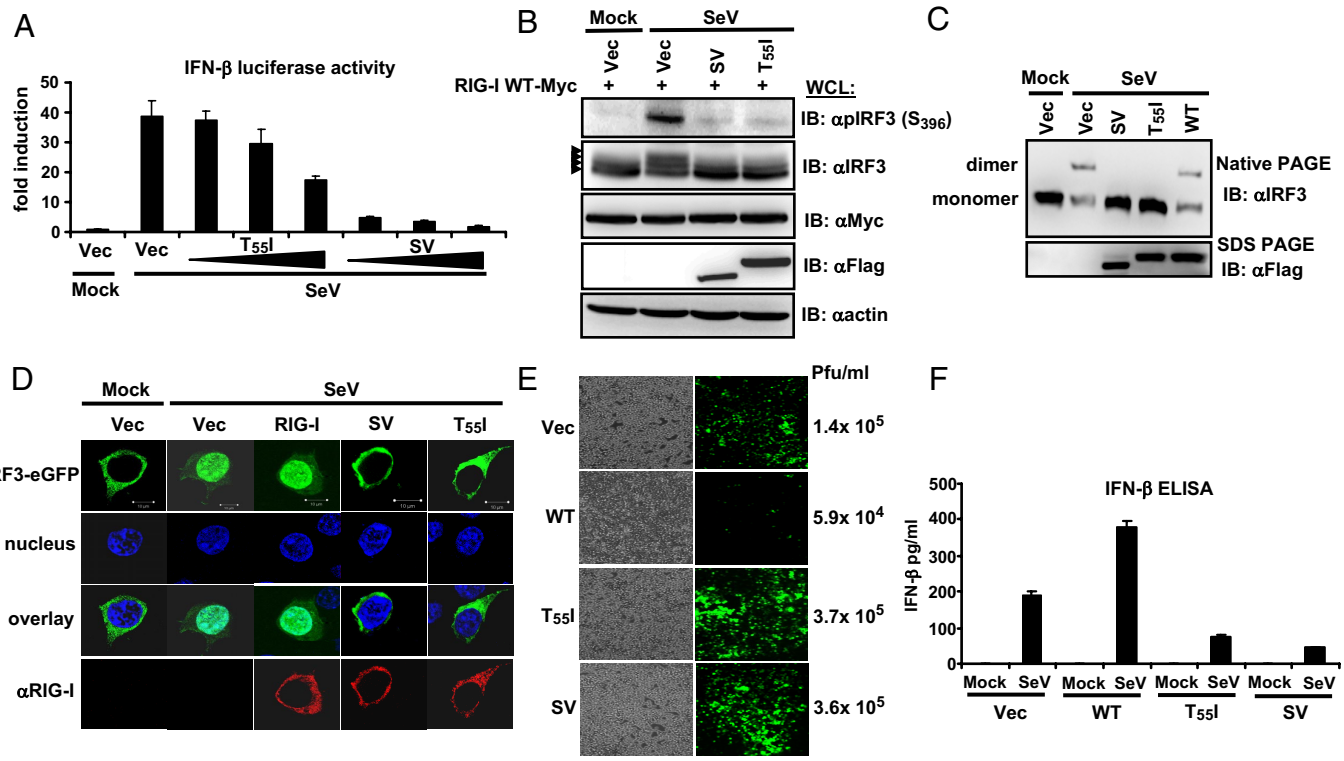

Fig. 4. RIG-I SV inhibits RIG-I-mediated antiviral signaling. (*A*) RIG-I SV inhibits the SeV-induced IFN-β promoter activation. HEK293T were transfected with vector or increasing amounts of RIG-I T_{55}I or RIG-I SV together with IFN-β luciferase and pGK-β-gal. At 24 h after transfection, cells were mock-treated or infected with SeV, and luciferase activity was determined as described in Fig. 1*D*. Data represent the mean ± SD ($n = 3$). RIG-I SV inhibits virus-induced IRF3 phosphorylation (*B*) and dimerization (*C*). (*B*) At 24 h after infection with Myc-RIG-I (10 μg), Flag-RIG-I SV (2 μg) or Flag-RIG-I T_{55}I (2 μg), cells were mock-treated or infected with SeV (50 HA units/ml) for 16 h. WCLs were subjected to IB with α-Phospho-IRF3 (Ser_{396}), α-IRF3, α-Myc, α-Flag, or α-actin. (*C*) At 24 h after transfection with Flag-IRF3, Flag-RIG-I WT, RIG-I SV, or RIG-I T_{55}I, cells were mock-treated or infected with SeV (50 HA units/ml) for 18 h. WCLs were used for native PAGE and subjected to IB with α-IRF3. (*D*) RIG-I SV inhibits the virus-induced nuclear translocation of IRF3. At 24 h after transfection with IRF3-eGFP, HEK293T stably expressing vector, Flag-RIG-I, Flag-RIG-I SV, or Flag-RIG-I T_{55}I were mock-treated or infected with SeV and stained with α-RIG-I (red) and Hoechst 33256 (nucleus). (*E*) RIG-I SV expression increases VSV-eGFP replication. HEK293T stably expressing vector, RIG-I, RIG-I SV, or RIG-I T_{55}I were infected with VSV-eGFP at MOI 0.5. At 24 h after infection, virus titer and replication were determined by plaque assay and GFP expression, respectively. (*F*) RIG-I SV suppresses virus-induced IFN-β production. HEK293T stably expressing vector, RIG-I, RIG-I SV, or RIG-I T_{55}I were infected with SeV (50 HA units/ml) for 20 h. IFN-β production was measured by ELISA. Data represent the mean ± SD ($n = 3$).

expressing RIG-I SV or RIG-I T_{55}I mutant showed reduced amounts of secreted IFN-β upon SeV infection compared with cells expressing vector or RIG-I WT (Fig. 4*F*). These results collectively indicate that the RIG-I SV acts as a dominant inhibitor of the RIG-I-mediated antiviral response, possibly serving as a negative-feedback mechanism.

Inhibition of RIG-I Multimerization and RIG-I-MAVS Signaling Complex Formation by RIG-I SV. To decipher the molecular mechanism of how the SV inhibits RIG-I-mediated IFN signal transduction, we tested RIG-I SV mutants in their ability to suppress the SeV-induced IFN induction: RIG-I SV K_{270}A mutant with the loss of ATPase activity (11) and RIG-I SV $C_{810,813}$A with the abolished RD structure (13). Although RIG-I SV and RIG-I SV K_{270}A strongly inhibited the SeV-induced IFN-β promoter activation, RIG-I SV $C_{810,813}$A did not show any significant inhibitory effect (Fig. 5*A*), indicating that the intact structure of the C-terminal RD is critical for the inhibitory effect of RIG-I SV.

The C-terminal RD of RIG-I specifically binds 5′-triphosphate viral RNA, and this interaction triggers RNA-dependent RIG-I dimerization. Therefore, the RIG-I SV was tested for its ability to bind 5′-triphosphate viral RNA and to interact with RIG-I WT. Fluorescence anisotropy analysis showed that RIG-I WT and RIG-I SV had similar binding affinities to *in vitro*-transcribed 5′-triphosphate containing rabies virus leader RNA (5′pppRVL): WT (K_d = 246.41 nM) and SV (K_d = 233.39 nM) (Fig. S9*A*). Furthermore, RIG-I SV readily interacted with RIG-I WT in the presence and absence of viral infection, and this interaction detectably inhibited RIG-I multimerization in a dose-dependent manner (Fig. 5 *B* and *C* and Fig. S9*B*). Finally, ectopic expression of the RIG-I SV and RIG-I T_{55}I led to a considerable reduction of RIG-I WT interaction with MAVS-CARD-PRD or full-length MAVS induced by SeV infection (Fig. 5*D* and Fig. S9*C*). These results indicate that the RIG-I SV interacts with RIG-I WT, and this interaction efficiently inhibits RIG-I multimerization and RIG-I-MAVS-interaction, resulting in a potent inhibition of virus-induced IFN signal transduction.

Discussion

A previous study (19) has shown that the naturally occurring T_{55}I mutation of the RIG-I first CARD in the hepatocyte Huh7.5 cells disrupts the signaling activity of the CARDs, resulting in a high permissiveness to HCV replication. Our data revealed that the T_{55}I mutation of the RIG-I first CARD completely abolished its ability to bind TRIM25, leading to the loss of RIG-I CARD ubiquitination and signaling activity.

The essence of the intact tandem CARD for RIG-I ubiquitination-dependent activity is further evidenced by the identification of a novel RIG-I SV whose expression is induced upon viral infection or IFN stimulation. Because of a short deletion in its first CARD, the RIG-I SV is unable to carry out TRIM25 interaction, ubiquitination, and, ultimately, antiviral signal transduction. Besides its lack of signaling activity, this SV acts as an endogenous inhibitor of

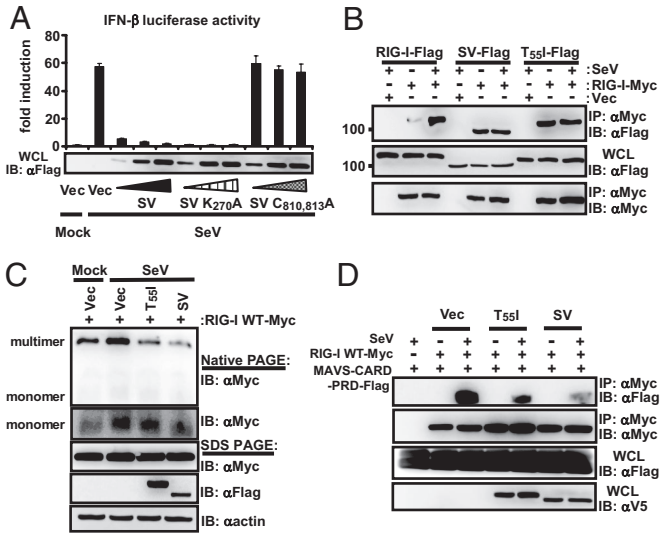

Fig. 5. RIG-I splice variant inhibits virus-induced RIG-I multimerization and RIG-I-MAVS complex formation. (*A*) The important role of the C-terminal RD of RIG-I splice variant for its inhibitory activity. After transfection with vector, RIG-I SV, or its mutants (K_{270}A or $C_{810,813}$A) together with IFN-β luciferase and pGK-β-gal, HEK293T cells were mock-infected or infected with SeV (50 HA units/ml) for 15 h. Data represent the mean ± SD ($n = 3$). (*B*) RIG-I splice variant interacts with RIG-I WT. After transfection with Flag-RIG-I WT, Flag-RIG-I SV, or Flag-RIG-I T_{55}I together with Myc-RIG-I WT, HEK293T were mock-infected or infected with SeV (50 HA units per ml) for 15 h and WCLs were used for IP with α-Myc, followed by IB with α-Flag. (*C*) RIG-I splice variant interferes with virus-induced RIG-I multimerization. Upon expression of Flag-RIG-I SV or RIG-I T_{55}I, Myc-RIG-I WT multimerization was determined by IB with α-Myc in native PAGE. To detect RIG-I monomer, the lower part of the membrane was exposed for a longer period of time (second from top). (*D*) RIG-I splice variant inhibits RIG-I-MAVS-interaction. HEK293T were cotransfected with MAVS-CARD-PRD-Flag and Myc-RIG-I WT together with vector, V5-RIG-I SV, or V5-RIG-I T_{55}I and subsequently either mock-treated or infected with SeV (50 HA units per ml) for 15 h. WCLs were subjected to IP with α-Myc, followed by IB with α-Flag.

RIG-I signal transduction, possibly providing a negative-feedback inhibition or fine-tuning mechanism.

The RIG-I C-terminal RD contains the highly conserved Cys_{810}-, Cys_{813}-, Cys_{864}-, and Cys_{869}-comprising zinc-coordination site as a key structural element for its functional activities (13). Our data showed that the structural integrity of the RD is critical for the inhibitory activity of the RIG-I SV, because the $C_{810,813}$A mutant no longer inhibited virus-induced IFN signal transduction. Upon binding to viral RNA, the RIG-I RD triggers a structural switch to induce the RNA-dependent RIG-I dimerization (13). Because RIG-I WT and the RIG-I SV exhibited similar binding affinities to 5′-triphosphate RNA, viral RNA-sequestration may not serve as the main mechanism of the inhibitory effect of the RIG-I SV on virus-induced IFN signal transduction. The RIG-I SV, instead, efficiently interacted with RIG-I WT to form a RIG-I WT-RIG-I SV heterocomplex, and this interaction suppressed RIG-I WT multimerization as well as RIG-I-MAVS interaction that are critical for RIG-I signaling.

Cui *et al.* (13) have suggested a potential model for the C-terminal RD-dependent RIG-I activation. In the absence of viral infection, RIG-I is monomeric and inactive by masking the central DECH domain with its N-terminal CARDs. Upon viral 5′ ppRNA interaction, the RD undergoes a conformational change and dimerizes, displacing the CARDs. Our study also suggests the multiple steps of the N-terminal CARD-dependent RIG-I activation. Upon viral RNA binding, the RIG-I first CARD is exposed and binds TRIM25 that subsequently ubiquitinates the lysine residues of the RIG-I second CARD. The ubiquitinated RIG-I CARDs effectively interact with MAVS, eliciting downstream antiviral signal transduction to induce IFN-α/β production.

Materials and Methods

Native PAGE. Native PAGE was performed by using a 7.5% acrylamide gel (Bio-Rad). The gel was prerun with 25 mM Tris and 192 mM glycine (pH 8.4) with or without 0.7% deoxycholate in the cathode and anode chamber, respectively, for 30 min at 30 mA. Samples in the native sample buffer [62.5 mM Tris·HCl (pH 6.8), 15% glycerol] were applied on the gel and electrophoresed for 40–80 min at 10 mA, followed by immunoblotting.

Confocal Immunofluorescence Microscopy. Cell preparation and confocal microscopy analysis were performed as described (20).

Other methods and materials are provided as *SI Text*.

ACKNOWLEDGMENTS. This work was partly supported by U.S. Public Health Service Grants CA82057, CA91819, CA31363, CA106156, and RR00168 (to J.U.J.), GM065367 (to T.J.), the graduate training programs 1071 (M.U.G.) and 1102 (A.K.), and the German Research Council Program Project 455 (K.P.H.).

1. Hiscott J, Lin R, Nakhaei P, Paz S (2006) MasterCARD: A priceless link to innate immunity. *Trends Mol Med* 12:53–56.
2. Akira S, Uematsu S, Takeuchi O (2006) Pathogen recognition and innate immunity. *Cell* 124:783–801.
3. Meylan E, Tschopp J, Karin M (2006) Intracellular pattern recognition receptors in the host response. *Nature* 442:39–44.
4. Creagh EM, O'Neill LA (2006) TLRs, NLRs and RLRs: A trinity of pathogen sensors that co-operate in innate immunity. *Trends Immunol* 27:352–357.
5. Hornung V, *et al.* (2006) 5′-Triphosphate RNA is the ligand for RIG-I. *Science* 314:994–997.
6. Pichlmair A, *et al.* (2006) RIG-I-mediated antiviral responses to single-stranded RNA bearing 5′-phosphates. *Science* 314:997–1001.
7. Girardin SE, *et al.* (2003) Nod1 detects a unique muropeptide from Gram-negative bacterial peptidoglycan. *Science* 300:1584–1587.
8. Girardin SE, *et al.* (2003) Nod2 is a general sensor of peptidoglycan through muramyl dipeptide (MDP) detection. *J Biol Chem* 278:8869–8872.
9. Kawai T, Akira S (2007) Antiviral signaling through pattern recognition receptors. *J Biochem* 141:137–145.
10. Garcia-Sastre A, Biron CA (2006) Type 1 interferons and the virus–host relationship: A lesson in detente. *Science* 312:879–882.
11. Yoneyama M, *et al.* (2004) The RNA helicase RIG-I has an essential function in double-stranded RNA-induced innate antiviral responses. *Nat Immunol* 5:730–737.
12. Saito T, *et al.* (2007) Regulation of innate antiviral defenses through a shared repressor domain in RIG-I and LGP2. *Proc Natl Acad Sci USA* 104:582–587.
13. Cui S, *et al.* (2008) The C-terminal regulatory domain is the RNA 5′-triphosphate sensor of RIG-I. *Mol Cell* 29:169–179.
14. Takahasi K, *et al.* (2008) Nonself RNA-sensing mechanism of RIG-I helicase and activation of antiviral immune responses. *Mol Cell* 29:428–440.
15. Seth RB, Sun L, Ea CK, Chen ZJ (2005) Identification and characterization of MAVS, a mitochondrial antiviral signaling protein that activates NF-kappaB and IRF 3. *Cell* 122:669–682.
16. Kawai T, *et al.* (2005) IPS-1, an adaptor triggering RIG-I- and Mda5-mediated type I interferon induction. *Nat Immunol* 6:981–988.
17. Meylan E, *et al.* (2005) Cardif is an adaptor protein in the RIG-I antiviral pathway and is targeted by hepatitis C virus. *Nature* 437:1167–1172.
18. Xu LG, *et al.* (2005) VISA is an adapter protein required for virus-triggered IFN-beta signaling. *Mol Cell* 19:727–740.
19. Sumpter R, Jr, *et al.* (2005) Regulating intracellular antiviral defense and permissiveness to hepatitis C virus RNA replication through a cellular RNA helicase, RIG-I. *J Virol* 79:2689–2699.
20. Gack MU, *et al.* (2007) TRIM25 RING-finger E3 ubiquitin ligase is essential for RIG-I-mediated antiviral activity. *Nature* 446:916–920.
21. Arimoto K, *et al.* (2007) Negative regulation of the RIG-I signaling by the ubiquitin ligase RNF125. *Proc Natl Acad Sci USA* 104:7500–7505.
22. Rothenfusser S, *et al.* (2005) The RNA helicase Lgp2 inhibits TLR-independent sensing of viral replication by retinoic acid-inducible gene-I. *J Immunol* 175:5260–5268.
23. Komuro A, Horvath CM (2006) RNA- and virus-independent inhibition of antiviral signaling by RNA helicase LGP2. *J Virol* 80:12332–12342.
24. Rosenstiel P, *et al.* (2006) A short isoform of NOD2/CARD15, NOD2-S, is an endogenous inhibitor of NOD2/receptor-interacting protein kinase 2-induced signaling pathways. *Proc Natl Acad Sci USA* 103:3280–3285.
25. Leung E, Hong J, Fraser A, Krissansen GW (2007) Splicing of NOD2 (CARD15) RNA transcripts. *Mol Immunol* 44:284–294.
26. Janssens S, Burns K, Tschopp J, Beyaert R (2002) Regulation of interleukin-1- and lipopolysaccharide-induced NF-kappaB activation by alternative splicing of MyD88. *Curr Biol* 12:467–471.